Mon. Not. R. Astron. Soc. **000**, 000–000 (0000) Printed 13 August 2003 (MN LaTeX style file v1.3)

Velocity-Delay Maps of Broad Emission Lines in Mrk 110

Keith Horne[1], Kollatschny, W.[2], (Welsh, W.F.?)
[1] *Physics and Astronomy, University of St. Andrews, KY16 9SS, Scotland, UK*
(`kdh1@st-and.ac.uk`*)*
[2] *Universitäts-Sternwarte Göttingen, Greismarlandstraβe 11, D-37083 Göttingen, Germany*
(`wkollat@uni-sw.dwdg.de`*)*

Accepted . Received ; in original form

ABSTRACT

We present velocity-delay maps for Balmer, He I, and He II emission from the active nucleus of the Seyfert 1 galaxy Mrk 110 based on spectral variations observed with the 9.2 m *HET* at Mc Donald Observatory.

Key words: (??)

1 INTRODUCTION

The correlation between black hole mass and the properties of the bulge stellar population in nearby galaxies (macgorian,ferrarese) indicates that nuclear black holes are intimately connected with the formation and evolving structure of their host galaxies. Masses for black holes in nearby galactic nuclei can be estimated from observations of stellar velocity distributions at small angular separations from the nucleus (refs). This technique works well for nearby galaxies, but becomes difficult for more distant galaxies and for galaxies with active nuclei (AGN).

In Seyfert 1 galaxies exhibiting Broad Emission-line Regions (BLR), black hole masses can be estimated from measurments of the emission-line velocity dispersion, and time delays from monitoring continuum and emission line flux variations (refs). The emission line variations lag behind those seen in the continuum, the lines being driven by photoionisation, and the delays arising from light travel time. These reverberation masses are generally in good agreement, (ferrarese) and enable the method to be extended to much greater distances. Indeed, by using reverberation masses to calibrate secondary mass estimators (Peterson,Wandel,..), a method analogous to distance ladder techniques, the black hole masses can be estimated at large redshifts to assist in population studies of the growth and evolution of black holes and their host galaxies (ref).

While substantial evidence for the presence of virial motions validates the use of this assumption in deriving black hole masses (petererson), the results are still relatively crude because the detailed geometry and kinematics of the BLR gas is not well understood (krolik). One set of models envisions the gas arising from an accretion disk wind, driven either magnetically (Blandford & Payne 2003; Bottorof, et al. 1997) or by radiation pressure (Chiang & Murray 1996; Proga, Stone, Kallman 2000). Alternatively, galactic centres are often the sites of bursts of star formation, and the nuclear black holes thereby attract tight star clusters that interact dynamically with the black hole. Our own galactic centre is a good example (ref). The BLR gas may have a more isotropic velocity distribution if it arises from debris stripped or evaporated from the obiting stars. The reverberation masses are uncertain by factors of order 3 due to the uncertain geometry.

The geometry and kinematics of the BLR can be probed by using the observed spectral variations to construct velocity-delay maps of the emission-line gas (refs). The velocity-delay distribution is strongly dependent on the nature of the flow (Welsh & Horne 1991; Perez, Robinson, de la Fuente 1992). This technique achieves micro-arcsecond resolution, and may help to discriminate among various models currently under consideration. The method has been used to construct velocity-delay maps of C IV 1550å emission based on *IUE* observations of NGC 4151 (Ulrich & Horne 1996), and *HST* observations of NGC 5548 (Done & Krolik 1996). The maps are generally consistent with virial motion, and rule out BLR models with purely radial motion. The delay resolution of these maps is of order 5-10 days, limited by the number of spectra (typically ~ 50) and systematic errors in the *IUE* and early *HST* spectrophotometry ($\approx 2-3\%$). This is typical of most of the AGN monitoring campaigns undertaken to date. As a consequence, the velocity-delay maps are not yet sharp enough to cleanly discriminate among several competing BLR models.

With the advent of robotic and queue-scheduled spectroscopy on ground-based telescopes, sustained monitoring of AGNs may soon become more routine. There is also some possibility that as the *HST* approaches the climax of its active life it will be used in a relatively low-cost observing mode for sustained monitoring of selected targets, as was the case with *IUE.* These opportunities may enable substantially improve resolution of velocity-delay maps of AGNs.

The delay resolution improves roughly in proportion to the duration and signal-to-noise ratio of the observations, up to a limit set by the time resolution. Assuming that post-calibration systematic errors can be kept at or below 1/monitoring sustained for 200 days. Ground-based monitoring will be limited to optical lines, but parallel /hst/ observations could provide ultraviolet lines needed for 5-dimensional mapping (Horne, Korista, Goad 2003). The proposed *Kronos* mission would routinely deliver micro-arcsecond velocity-delay maps for a variety of ultraviolet and optical lines, with time-lapse mapping capabilities to track fine structures such as spiral wave patterns on AGN disks or debris trails behind individual stars.

In this paper we construct velocity-delay maps for the optical emission lines in Mrk 110 based on a 26-epoch campaign of spectroscopic *HET* observations. Section 2 summarises the *HET* observations, data reduction, and previous cross-correlation analysis. Section 3 fits a reverberation model to the observed spectral variations to derive velocity-delay maps for the emission lines. Section 3 discusses the results, and Section 3 summarises the main conclusions.

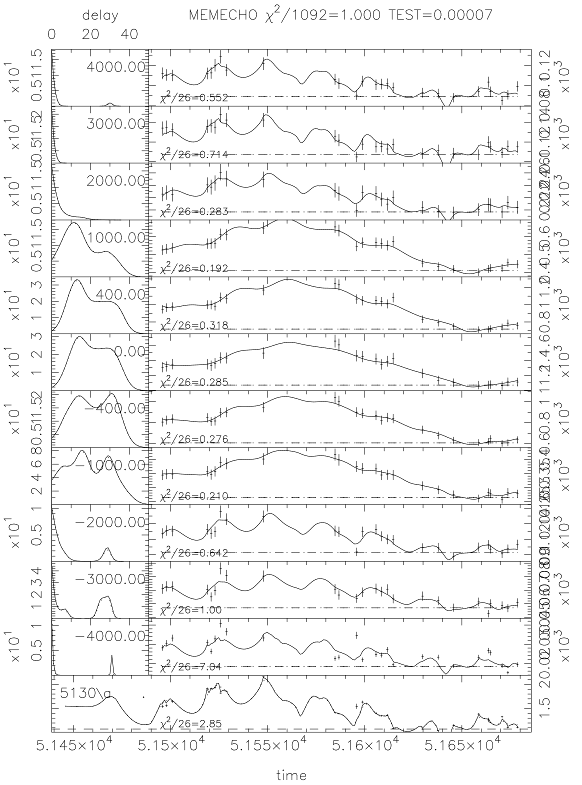

Figure 1. MEMECHO fit to continuum measurements (bottom) and velocity-resolved emission-line measurements (top right) deterine delay maps for each velocity bin (top left). This fit to the Hβ emission line achieves $\chi^2/N = 1$.

2 OBSERVATIONS AND CROSS-CORRELATION ANALYSIS

The observations taken with the *HET* are described elsewhere (Kollatschny 2003). Briefly, these consist of 26 spectra taken with the LRS spectrograph at the prime focus of the *HET* obtained on 26 nights during the 183-day interval 1999 Nov 13 to 2000 May 14. The mean and median time sampling are 7.3 and 3.0 days, respectively. The spectra cover 4200å to 6900å with a velocity resolution of 460 km s^{-1} at 5000 å.

The data reduction is also described elsewhere (Kollatschny 2003). The observed spectra were corrected for small instrumental and seeing-induced pixel shifts and blurring, and then renormalized to make the fluxes of narrow emission lines constant in time. After transformation to the emitted frame, a pseudo-continuum was fitted to each spectrum, and lightcurves were extracted by summing over selected wavelength intervals to sample the continuum at several wavelengths, and emission lines in velocity bins. A common velocity grid with a velocity of either $\Delta V = 200$ km s^{-1} or $\Delta V = 400$km s^{-1} was used for the Hα, Hβ, He I 5876å, and He II 4686å, emission lines.

A cross-correlation analysis of these lightcurves (Kollatschny 2003) has already revealed evidence for virial motions, estimates for the black hole mass, $M \sin i \approx 2 \times 10^7 M_\odot$, and longer delays in the red wing of the line suggesting that the broad emission lines arise from an accretion disc wind. The velocity-resolved cross-correlation function between emission-line and continuum lightcurves is

$$CCF(V,\tau) = \int \eta_c(t-\tau)\ \eta_\ell(V,t)\ \mathrm{d}t\ , \tag{1}$$

where $\eta_c(t)$ and η_ℓ are normalized versions of the continuum and velocity-resolved emission-line lightcurves, respectively, e.g., interpolated from the observations. The average time delay, or 'lag', is defined by

$$\langle\tau\rangle = \int_{\tau_1}^{\tau_2} \tau\ \mathrm{d}\tau \int \mathrm{d}V\ CCF(V,\tau)\ , \tag{2}$$

averaging over a delay range τ_1 to τ_2 bracketing the peak of the cross-correlation peak. Assuming that the time delays arise principally from light-travel time, the measurement of $\langle\tau\rangle$ estimates the size of the emission-line region,

$$\langle R\rangle = c\,\langle\tau\rangle\ , \tag{3}$$

with c the speed of light. The measured delays correlate inversely with the velocity dispersion of the variable component of the emission-line flux, $\langle\tau\rangle \propto 1/\left\langle V^2\right\rangle$, consistent with and providing evidence for virial motions. The black hole mass is then estimated via

$$M = \frac{f\,c}{G}\left\langle V^2\right\rangle\langle\tau\rangle\ , \tag{4}$$

with G the gravitational constant and f a fudge factor depending on the uncertain geometry of the virial flow, e.g., $f \propto \sin i$ for a Keplerian disk at inclination angle i.

3 VELOCITY-DELAY MAPS

The velocity-delay maps $\Psi(V,\tau)$ describe spectral variations $f(\lambda,t)$ in terms of delayed responses to variations in a 'driving' lightcurve $X(t)$.

$$f(V,t) = b(\lambda) + \int_0^{\tau_{\max}} \Psi(V,\tau)\ X(t-\tau)\ \mathrm{d}\tau\ . \tag{5}$$

In this reverberation model, the time-independent 'background' spectrum, $b(\lambda)$ accounts for steady light sources, such as starlight and emission from regions too large to reverberate on the monitoring timescale. For the maximum time delay, $\tau_{\max}$, we adopt 50 days, about 1/3 of the duration of the monitoring observations. For the 'driving lightcurve', $X(t)$, we adopt a fit to the observed variations in the continuum at 5130å

$$X(t) = f_c(t) - f_0 \ , \qquad (6)$$

where we subtract a constant f_0, taken to be flux exceeded by 95% of the continuum measurements.

We have used the MEMECHO code (Horne, Welsh, Peterson 2003; Horne 2003; Ulrich & Horne 1996) to fit the above reverberation model to the observed spectral variations. The fit adjusts the driving lightcurve $X(t)$, the background spectrum $b(\lambda)$, and the velocity-delay map $\Psi(V,\tau)$. The fit attempts to minimize χ^2, but is regularized by a maximum entropy criterion designed to deliver, roughly speaking, the 'smoothest' functions that fit the data at specified levels of χ^2. Fig. 1 shows a representative fit to the observed lightcurves in selected velocity bins across the Hβ profile.

We have constructed maps $\Psi(V,\tau)$ for 5 emission lines, Hα, Hβ, Hβ, He I 5876å, and He II 4686å. Fig. 2 shows one map for each line, while Figs. 4 thru 7 show 9 maps for each line, to illustrate the trade-off between noise and resolution, and between smearing in v vs τ.

For each line we have constructed 18 maps, considering two different velocity binnings, $\Delta V = 200$ km s^{-1} and $\Delta V = 400$ km s^{-1}, 3 different χ^2 levels, $\chi^2/N = 1$, 1.5, and 2, and 3 different values of a control parameter, $A = 0$, 0.1, and 1. When the control parameter A is 0, there is no connection between adjacent velocity bins, and the entropy makes $\Psi(V,\tau)$ 'as smooth as possible' in the τ direction. For $a = 0.1$ there is a mild connection between adjacent velocity bins, and for $a = 1$ the connection is stronger, causing the maps to become smoother in v and less smooth in τ.

4 DISCUSSION

5 CONCLUSION

REFERENCES

Blandford, R.D., Payne, D.G. 1982, MNRAS, 199, 883.
Bottorof, M., Korista, K.T., Shlosman, I., Blandford, R.D. 1997, ApJ, 479, 200.
Chiang, J., Murray, N. 1996, ApJ, 466, 704.
Done, C., Krolik, J.H. 1996, ApJ, 463, 144.
Horne, K., Welsh, W.F, Peterson, B.M. 1991, ApJ 367, L5.
Horne, K., 1994, ASP Conf. Ser. 69, 23.
Horne, K., Korista, K.T., Goad, M.R. 2003, MNRAS, 339, 367.
Kollatschny, W., Bischoff, K., Robinson, E.L, Welsh, W.F. Hill, G.J. 2001, A&A, 379, 125.
Kollatschny, W., 2003, A&A, 407, 461.
Perez, E., Robinson, A., de la Fuente, L. 1992, MNRAS, 256, 103.
Proga, D., Stone, J.M., Kallman, T.R. 2000, ApJ, 543, 686.
Ulrich, M.-H., Horne, K., 1996, MNRAS, 283, 748.
Welsh, W.F., Horne, K., 1991, ApJ, 379, 586.

This paper has been produced using the Royal Astronomical Society/Blackwell Science LaTeX style file.

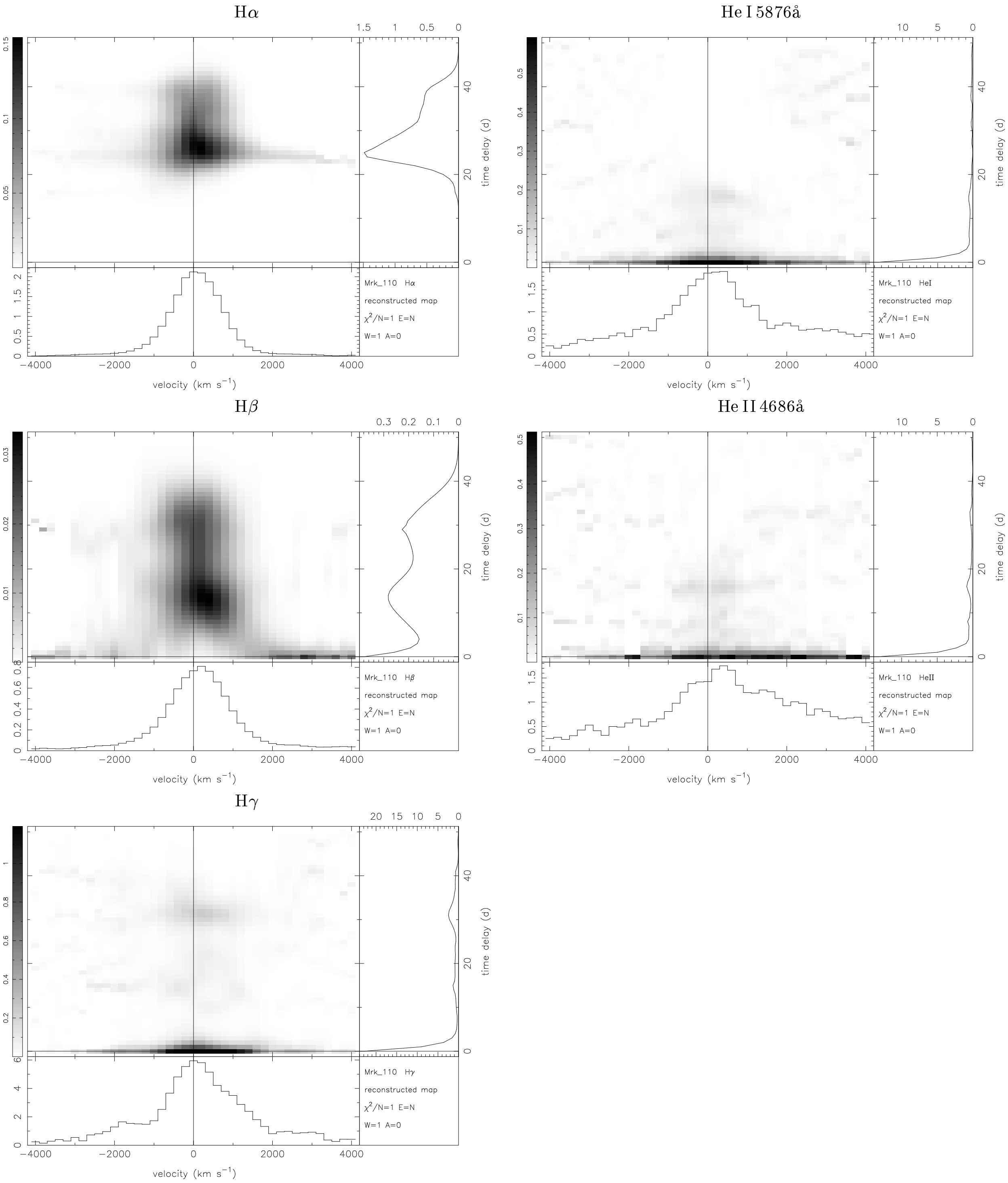

Figure 2. Velocity-delay maps $\Psi(V,\tau)$ for optical emission lines in Mrk 110. The velocity and delay resolution are $\Delta v = 200$ km s^{-1} and $\Delta\tau = 1$ d, and the maps are for $\chi^2/N = 1$ and $A = 0$.

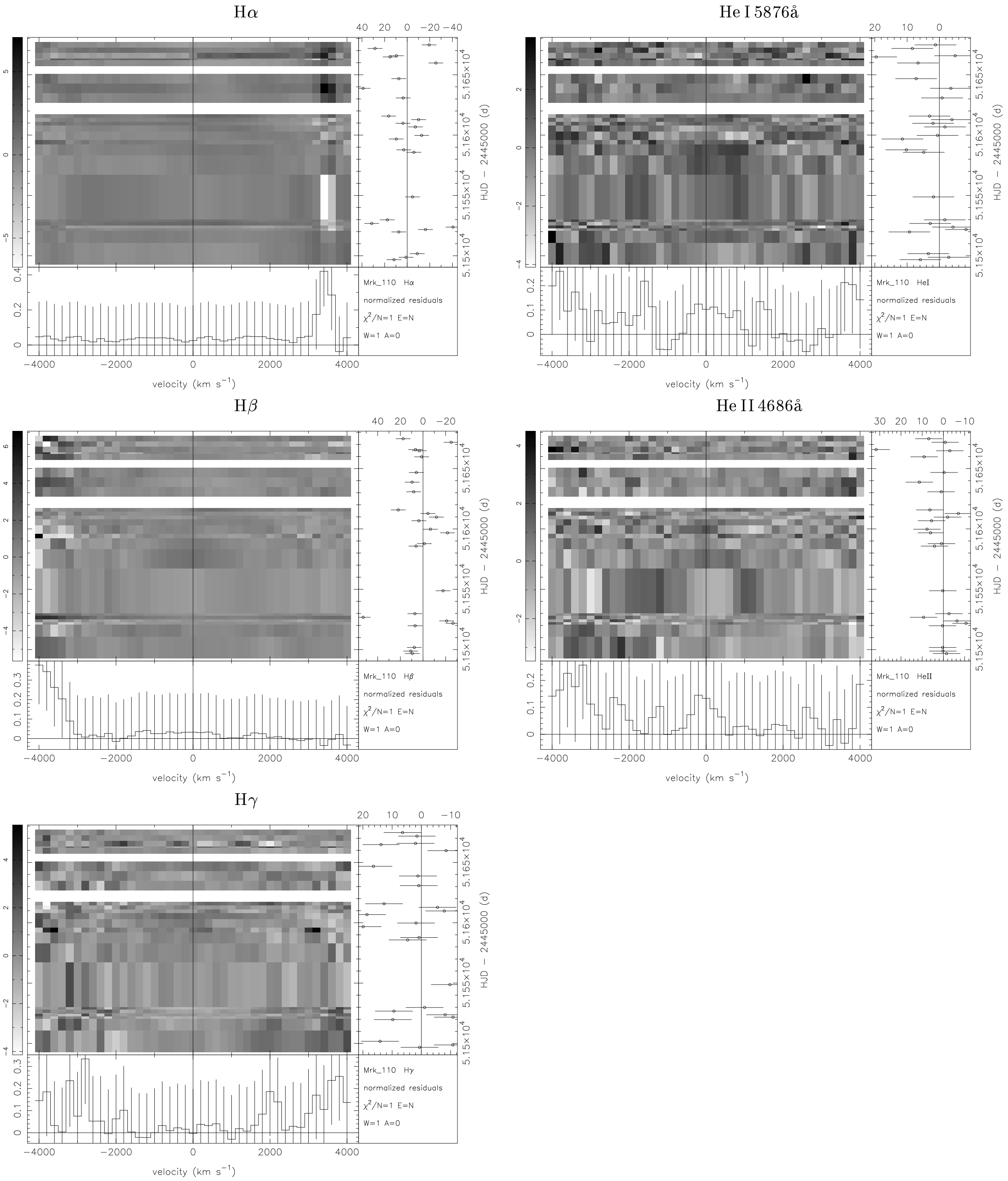

Figure 3. Normalized residuals of the MEMECHO fit as a function of velocity and time for each of the emission lines in Fig. 2.

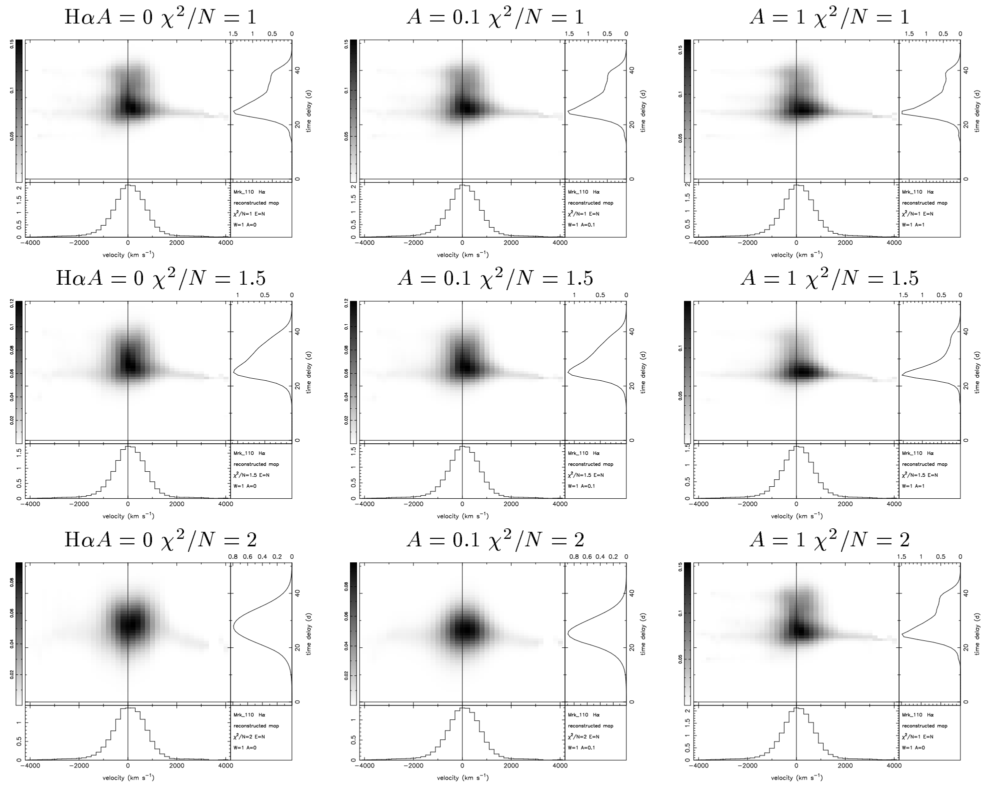

Figure 4. Hα velocity-delay maps $\Psi(V, \tau)$ with $\Delta v = 200$ km s^{-1} $\Delta\tau = 1$ d. Columns vary $\chi^2/N = 1, 1.5, 2$ and rows vary $A = 0, 0.1, 1$.

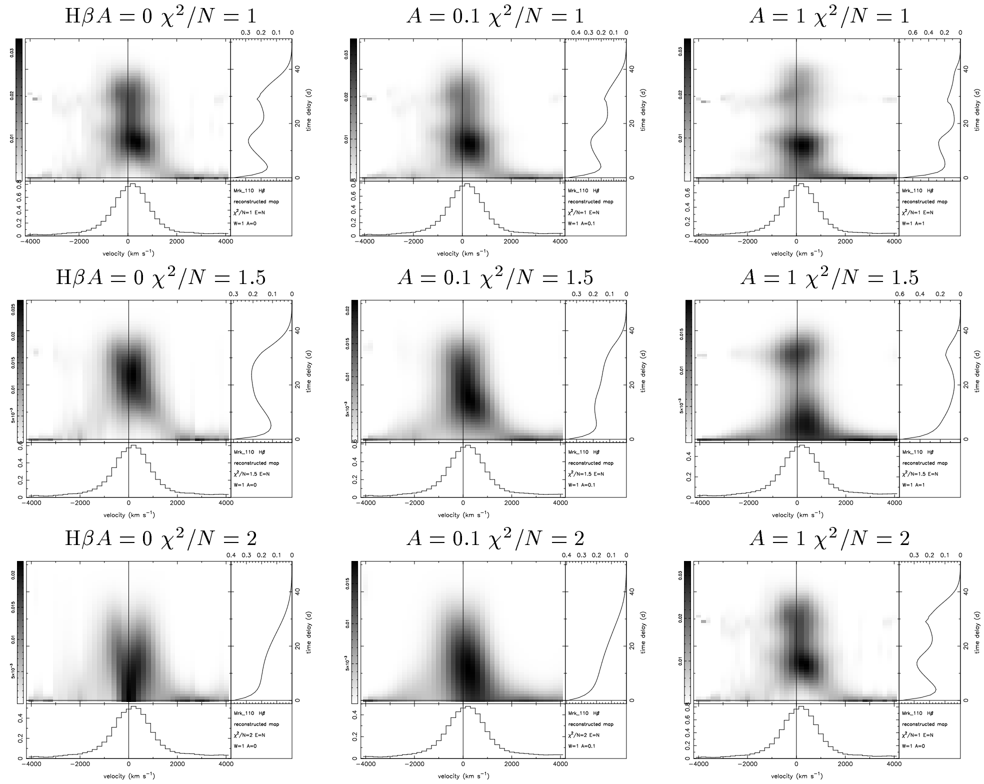

Figure 5. Hβ velocity-delay maps $\Psi(V, \tau)$ with $\Delta v = 200$ km s^{-1} $\Delta\tau = 1$ d. Columns vary $\chi^2/N = 1, 1.5, 2$ and rows vary $A = 0, 0.1, 1$.

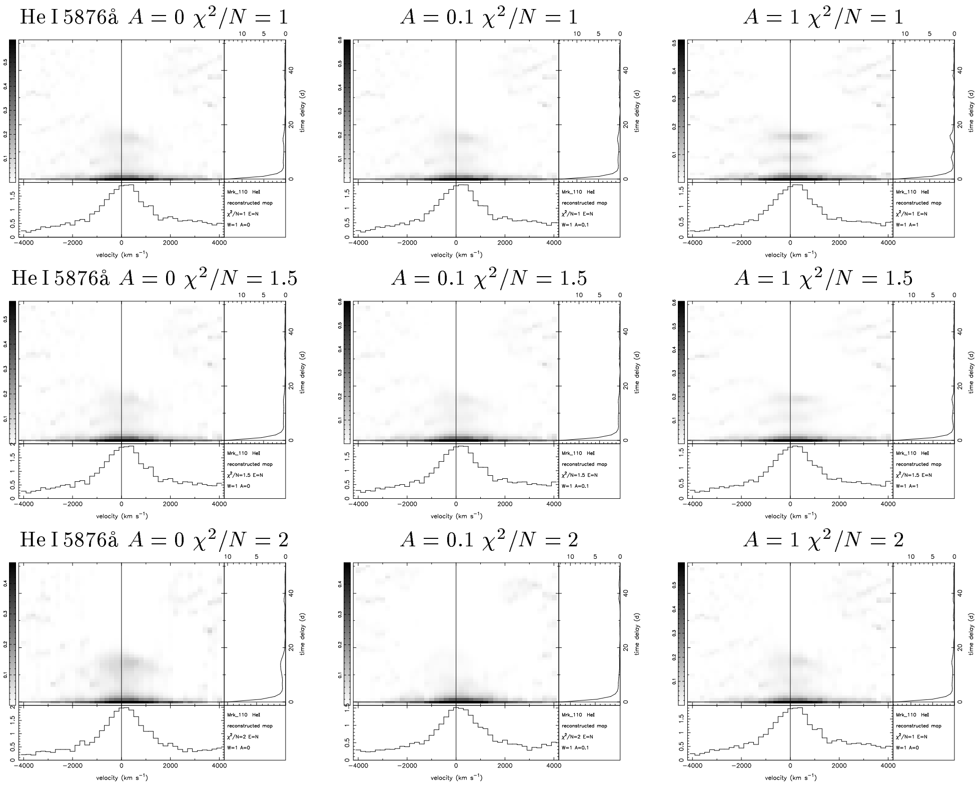

Figure 6. He I 5876å velocity-Delay maps $\Psi(V, \tau)$ with $\Delta v = 200$ km s^{-1} $\Delta\tau = 1$ d. Columns vary $\chi^2/N = 1, 1.5, 2$ and rows vary $A = 0, 0.1, 1$.

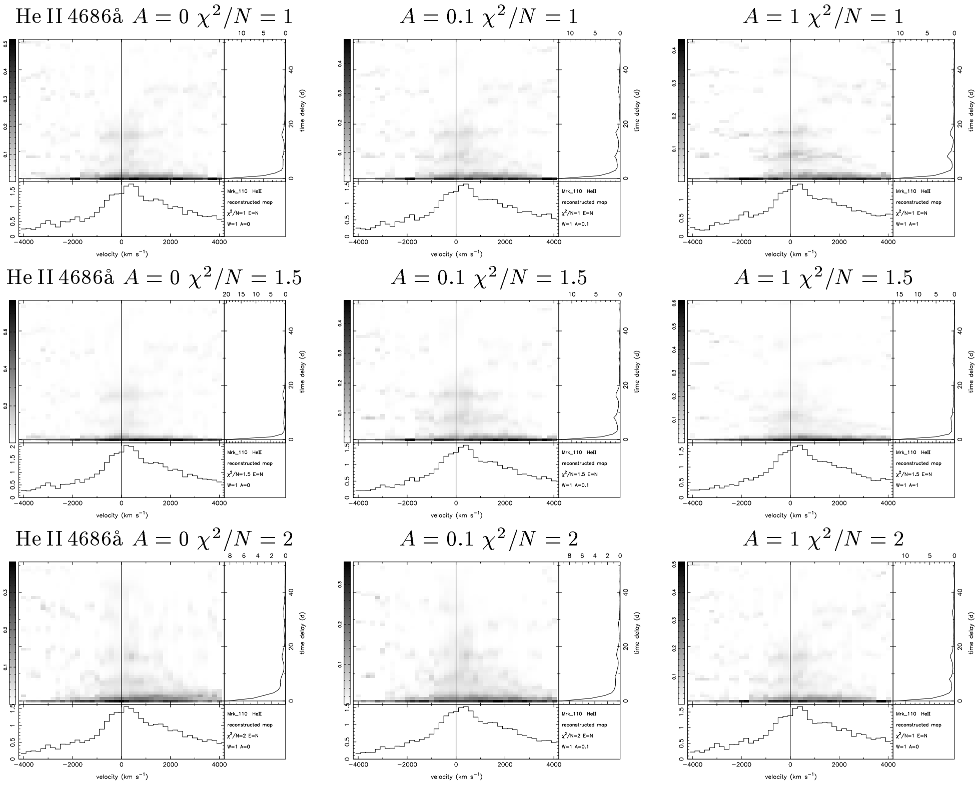

Figure 7. He II 4686å velocity-Delay maps $\Psi(V, \tau)$ with $\Delta v = 200$ km s^{-1} $\Delta\tau = 1$ d. Columns vary $\chi^2/N = 1, 1.5, 2$ and rows vary $A = 0, 0.1, 1$.